Journal of Molecular Structure 1289 (2023) 135847

Contents lists available at ScienceDirect

Journal of Molecular Structure

journal homepage: www.elsevier.com/locate/molstr

Reactive imines: Addition of 2-aminopyrimidine to the imine bond and isolation of the aminal from the equilibrium mixture aminal/imine

Magdalena Siedzielnik, Andrzej Okuniewski, Kinga Kaniewska-Laskowska, Marcin Erdanowski, Anna Dołęga *

Department of Inorganic Chemistry, Gdańsk University of Technology, Narutowicza 11/12, Gdańsk 80-233, Poland

ARTICLE INFO

Keywords:
Schiff bases
Aminal
VT NMR
Crystal structure
DFT calculations

ABSTRACT

The reaction between *o*-vanillin and 2-aminopyrimidine leads to the formation of a single crystalline product: aminal, **1**, which results from the reaction of the initially formed imine with 2-aminopyrimidine. The reaction was followed by the NMR spectroscopy. VT NMR studies prove that in solution two major species are observed: aminal and imine and their ratio depends on the time or/and temperature with the imine content increasing over time. One factor responsible for the non-typical course of the reaction between the aldehyde (*o*-vanillin) and 2-aminopyrimidine is the increased reactivity of the resulting imine, which easily undergoes nucleophilic addition. With the use of DFT calculations combined with experimental results we prove that the dual descriptor is the best parameter in predicting the increased reactivity of the imine bond. The calculations confirmed that the imine derived from *o*-vanillin and 2-aminopyrimidine is a reactive species. Another factor that determines the course of the reaction is relatively facile crystallization of aminal due to the extensive network of strong and weak hydrogen bonds. Several metal ions were tested as templating partners but no metal-imine complex could be isolated. Instead we have obtained and characterized structurally several metal ion complexes with *o*-vanillinate and 2-aminopyrimidine as ligands.

1. Introduction

Schiff bases are compounds of a great interest, as evidenced by the number of publications published annually on the topic within the last twenty years. Such a great interest can be explained by the fact that they are widely used in both organic and inorganic synthesis. The examples of organic syntheses include addition of nucleophiles and organometallic reagents to C═N bond *e.g.* [1–3], hetero Diels-Alder reaction [4], Staudinger reaction for the preparation of β-lactams [5] or potentially synthesis of β-aminoacids [6]. Inorganic chemistry applications include mainly syntheses of metal – imine complexes for separation/chelation of metal ions with their detection or further application as catalysts, SMM or corrosion inhibitors *e.g.* [7–14]. Moreover, imine bonds occur in many biologically active compounds used in medicine, analytical and pharmaceutical industry *e.g.* [12–17].

The special properties of Schiff bases are related both to the ease of synthesis as well as the properties of the compounds. Simultaneous presence of proton-donor and proton-acceptor groups creates the possibility of formation of inter- and intramolecular hydrogen bonds and participation in proton transfer processes [15,18,19]. The electrophilic carbon and nucleophilic nitrogen within the imine bond provide good binding properties with different nucleophiles and electrophiles. The imine nitrogen atom is acting as a Lewis base (electron donor) toward metal ions, thus, Schiff bases easily form complexes [20]. On the other hand, the reaction of imine bond formation is reversible and several follow-up reactions are possible thus the obtained imine compounds may undergo dynamic changes in solution. Such phenomena have been described and analyzed also lately, especially with regard to derivatives of heterocyclic nitrogen compounds, which seem to be especially susceptible to addition of nucleophiles [2,3,21,22].

Our work is the continuation of our study initiated few years ago in which we described the addition of methanol to the reactive imine bond of 2-methoxy-6-(4-pyridyliminomethyl)-phenol. Our initial goal *i.e.* syntheses of mono- or polynuclear complexes turned into the study on the reactivity of imines and we finally isolated the reactive imine by an indirect method and determined its distinct molecular structure [2]. Interestingly, isomers of the unstable imine were much less reactive and could be isolated and fully characterized and used for the synthesis of

* Corresponding author.
E-mail address: anna.dolega@pg.edu.pl (A. Dołęga).

https://doi.org/10.1016/j.molstruc.2023.135847
Received 14 February 2023; Received in revised form 12 May 2023; Accepted 22 May 2023
Available online 26 May 2023

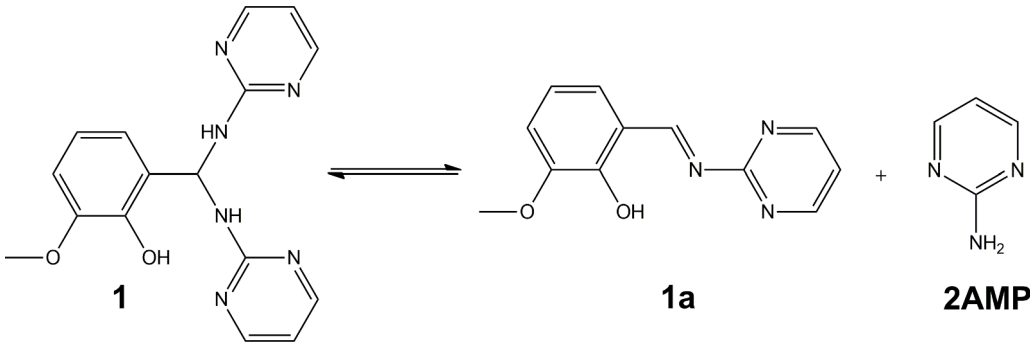

Scheme 1. Equilibrium reaction for **1** and **1a** in DMSO-d6.

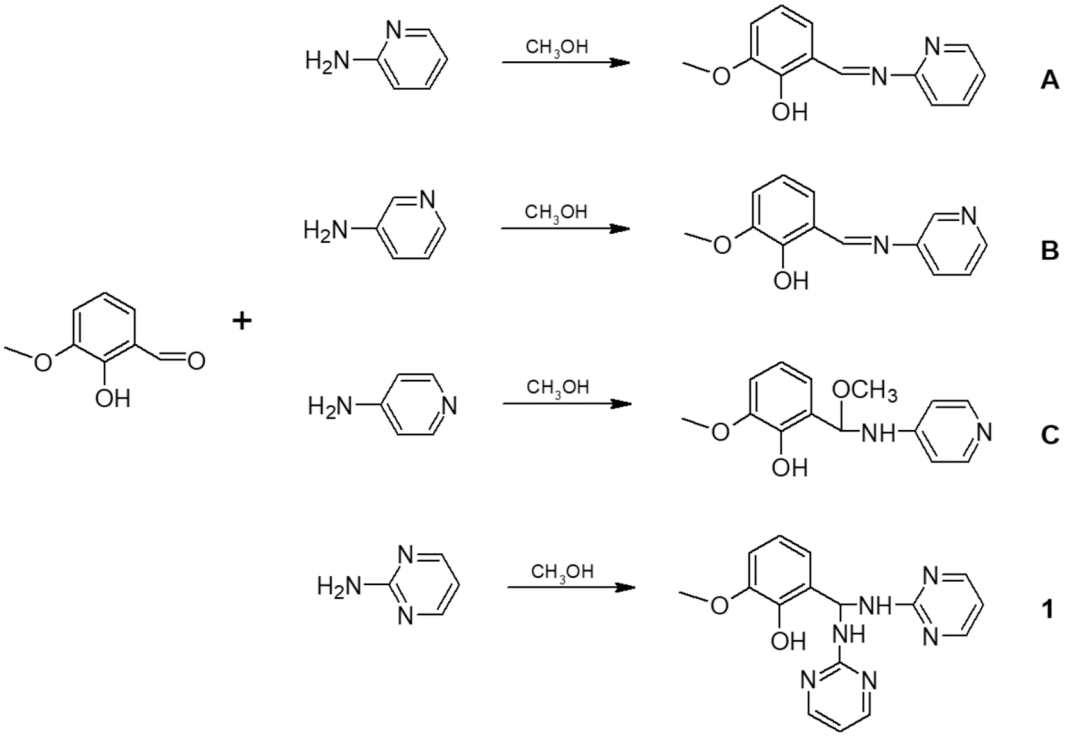

Scheme 2. Reactions of *o*-vanillin with isomeric aminopyridines and 2-aminopyrimidine. [2, this work].

metal complexes [23–25]. We tried to find a simple answer to the question why is the derivative of 4-AP so different with the regard to the reactivity and tried to explain the difference by quantum chemically calculated bond orders or HOMO–LUMO gaps [2]. Here we describe similar phenomenon for a different compound in the series: in the reaction of *o*-vanillin with 2-aminopyrimidine in methanol we invariably isolated aminal instead of the expected imine (Scheme 1 and 2). The attempts to produce the imine as a result of templating with metal ions were also unsuccessful (Scheme 3). In order to analyze the reactivity of aminopyridine/aminopyrimidine derivatives, we have DFT-optimized 14 geometries and analyzed several parameters that can be derived from the calculated electron density. Moreover, we performed aspherical crystal structure refinement for 2-(bis(pyrimidin-2-ylamino)methyl)-6-methoxyphenol and also used the resulting electron density to analyze the intermolecular interactions within the crystals of aminal.

2. Experimental

2.1. Synthesis of 2-(Bis-(pyrimidin-2-yl amino)-methyl)-6-methoxyphenol (1)

The methanolic solution (15 mL) of 0.951 g 2-aminopyrimidine (95.10 g/mol, 10.0 mmol) was added to the methanolic solution (15 mL) of 0.76 g *o*-vanillin (152.15 g/mol, 5.0 mmol). Afterwards the reaction mixture was heated under reflux for 3 h. On cooling to room temperature, changed of color was observed (from orange to yellow). Crystals were obtained after 1 day, at 277 K as colorless prisms. Yield of reaction 60.5 % (0.97 g). Elemental analysis: Calc. for $C_{16}H_{16}N_6O_2$: C: 59.25; H: 4.97; N: 25.91. Found: C: 59.10; H: 4.98; N: 25.17.

FT-IR: 3433(m, sh), 3217(m), 3174(m), 3134(m), 3102(m), 3062 (m), 3007(m), 2967(m), 2936(m), 2834(m), 1897(vw), 1662(vw), 1569 (s, sh), 1564(*vs*), 1536(s, sh), 1492(s), 1486(s), 1439(*vs*), 1423(s), 1409 (s), 1390(m), 1344(m), 1274(m), 1267(m), 1233(m), 1219(m), 1213(s), 1176(m), 1167(m), 1129(m), 1087(m), 1067(m), 1062(m), 987(w), 944 (m), 901(vw), 886(vw), 884(vw), 833(vw), 799(m), 787(w), 734(m, sh), 670(w), 641(w), 632(w), 587(vw), 557(vw), 553(w), 482(w), 480 (w), 410(vw) cm^{-1}

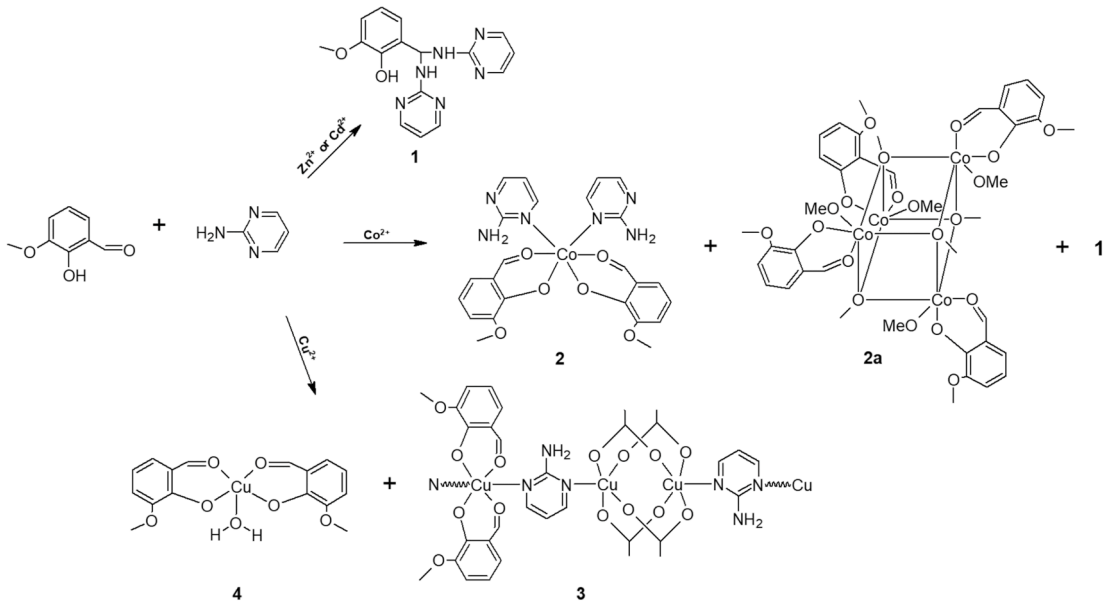

Scheme 3. Crystalline products of the reactions of o-vanillin with 2-aminopyrimidine and selected M(II) acetates.

NMR: ^{1}H NMR (DMSO-d_6, 400 MHz) δ 8.94 (1H, s, H-1 of OH), 8.29 (4H, d, J = 4.8 Hz, H-10, H-12, H-14, H-16), 7.22 (3H, s, overlapped signals of H-1A and H-4 of NH and H-8), 7.06 (1H, dd, J = 7.9, 1.2 Hz, H-5), 6.88 (1H, dd, J = 7.9, 1.2 Hz, H-3), 6.73 (1H, t, J = 7.9 Hz, H-4A), 6.62 (2H, t, J = 4.8 Hz, H-11, H-15), 3.79 (3H, s, H-7A, H-7B, H-7C of CH_3).

^{13}C{^{1}H} NMR (DMSO-d_6, 400 MHz) δ 161.4 (C, C-9, C-13), 158.4 (CH, C-10, C-12, C-14, C-16), 148.0 (C, C-2), 144.4 (C, C-1), 128.6 (C, C-6), 119.6 (CH, C-5), 118.9 (CH, C4), 111.6 (CH, C-3), 111.4 (CH, C-11, C-15), 58.2 (CH, C-8), 56.3 (CH_3, C-7).

It is important to note that in solution **1** remains in equilibrium with the 2-aminopyrimidine and Schiff base: 2-methoxy-6-(2-pyrimidyliminomethyl)-phenol. The variable temperature (VT) NMR spectra, which illustrate the equilibria, are discussed in the Results and Supplementary materials (chapter 3.1 and SI part S1).

2.2. Reactions of o-vanillin and 2-aminopyrimidine with metal acetates

2.2.1. Reaction with cobalt(II) acetate

The methanolic solution (15 mL) of 0.202 g 2-aminopyrimidine (95.10 g/mol, 2.14 mmol) and 0.311 g *o*-vanillin (152.15 g/mol, 2.04 mmol) was added to the methanolic solution (10 mL) of 0.249 g Co

Table 1
Experimental details.

Complex	1	2	3	4
Formula	$C_{16}H_{16}N_6O_2$	$C_{24}H_{24}CoN_6O_6$	$C_{32}H_{36}Cu_3N_6O_{14}$	$C_{16.48}H_{17.92}CuO_{7.48}$
Formula weight	324.35	551.42	919.29	399.29
Wavelength (Å)	0.71073	1.54186	0.71073	0.71073
Temperature (K)	120(2)	120(2)	120(2)	120(2)
Crystal system	Triclinic	Orthorhombic	Triclinic	Monoclinic
Space group	*P*-1	*Pna*2$_1$	*P*-1	*P*2$_1$/*c*
a (Å)	8.9874(19)	17.6358(5)	8.7680(6)	9.571(4)
b (Å)	9.599(2)	16.7257(4)	10.2279(8)	15.323(4)
c (Å)	11.003(4)	8.3415(2)	11.5222(9)	11.331(5)
α (°)	72.76(2)	90	80.035(6)	90
β (°)	83.90(2)	90	69.471(6)	99.42(4)
γ (°)	62.205(15)	90	77.407(6)	90
V (Å)	801.4(4)	2460.50(11)	939.10(13)	1639.4(11)
Z	2	4	1	4
Crystal size (mm)	0.16 × 0.10 × 0.06	0.60 × 0.24 × 0.06	0.13 × 0.11 × 0.10	0.10 × 0.09 × 0.08
T_{min}, T_{max}	0.990, 0.9996	0.224, 0.727	0.818, 0.891	0.868, 0.922
μ (mm^{-1})	0.094	5.923	1.757	1.372
Absorption correction	Integration	Integration	Integration	Integration
Reflections collected/unique/ unique(I > 2σ(I)]	7290/3134/2014	20,737/4193/3419	8136/3706/3340	9883/3222/2310
Completeness to 2θ=52°	0.995	0.989	0.999	0.999
R_{int}	0.0384	0.0522	0.019	0.036
Data/restraints/parameters	3134/0/230	4193/5/353	3706/0/97	3222/214/352
Goodness of fit (GOOF) on F^2	1.019	1.125	1.091	1.033
Final R indices (I > 2σ(I)]	R_1=0.0489	R_1=0.0475	R_1=0.0262	R_1=0.0451
	wR_2=0.1146	wR_2=0.1169	wR_2=0.0687	wR_2=0.0957
R indices (all data)	R_1=0.0881	R_1=0.0642	R_1=0.0305	R_1=0.0749
	wR_2=0.1308	wR_2=0.1369	wR_2=0.071	wR_2=0.1094
$\Delta\rho_{max}$, $\Delta\rho_{min}$ (e Å^{-3})	0.264 / − 0.247	0.417 / − 0.637	0.385 / − 0.258	0.304 / − 0.639
CCDC numbers	2241626	2241627	2241628	2241629

$(CH_3COO)_2{\cdot}4H_2O$ (249.08 g/mol, 1.0 mmol). The reaction mixture was heated under reflux for 30 minutes and then it was cooled to room temperature. The change of color was observed from pink to brown. Brown crystals of *(*bis(2-aminopyridine)bis(*o*-vanillinato-κ*O,O′*)cobalt (II)*)* (**2**) for X-ray diffraction analysis were obtained at 250 K.

The same reaction mixture but without prolonged heating produces as the main product cubic Co(II) *o*-vanillinate/methanolate complex [26]. The product was identify by X-ray diffraction (unit cell parameters) and FT-IR spectrum.

2.2.2. Reaction with copper(II) acetate

The 0.475 g 2-aminopyrimidine (95.10 g/mol, 5.00 mmol) and 0.760 g *o*-vanillin (152.15 g/mol, 5.00 mmol) were separately dissolved in 5 mL of hot methanol, mixed and added to the hot methanol/water solution (30 mL/5 mL) of 0.500 g $Cu(CH_3COO)_2{\cdot}H_2O$ (199.65 g/mol, 2.5 mmol). The reaction mixture was heated for 10 minutes and then it was cooled to room temperature. After mixing all reagents the immediate changed of color was observed from blue to green and crystallization began at RT. Blue-green crystals of two different complexes of Cu (II) **3** and **4** suitable for X-ray diffraction analysis were selected among the initial crystallization products.

2.2.3. Reaction with cadmium(II) acetate

The methanolic solution (10 mL) of 0.190 g 2-aminopyrimidine (95.10 g/mol, 2.00 mmol) and 0.304 g *o*-vanillin (152.15 g/mol, 2.00 mmol) was added to the methanol solution (10 mL) of 0.266 g $Cd(CH_3COO)_2{\cdot}2H_2O$ (266.53 g/mol, 1 mmol). The reaction mixture was heated for 10 min (it became orange), cooled to room temperature and left for slow evaporation. The colorless crystals that appeared after 24 h were identified as compound **1** (aminal) on the basis of X-ray diffraction and FT-IR spectroscopy.

2.2.4. Reaction with zinc(II) acetate

The 0.475 g 2-aminopyrimidine (95.10 g/mol, 5.00 mmol) and 0.760 g *o*-vanillin (152.15 g/mol, 5.00 mmol) were separately dissolved in 5 mL of hot methanol, mixed and added to the hot methanol the methanol solution (15 mL) of 0.548 g $Zn(CH_3COO)_2{\cdot}2H_2O$ (219.51 g/mol, 2.5 mmol). The reaction mixture was heated for 10 minutes (it became orange), cooled to room temperature and placed at 277 K. The colorless crystals that appeared after 24 hours were identified as compound **1** (aminal) on the basis of X-ray diffraction and FT-IR spectroscopy.

2.3. Refinement

Crystal data, data collection and structure refinement details are summarized in Table 1. The crystal structure data were collected on an IPDS 2T dual beam diffractometer (STOE & Cie GmbH, Darmstadt, Germany) at 120.0(2) K with $Mo_{K\alpha}$ radiation of a microfocus X-ray source – for **1, 3** and **4** (GeniX 3D Mo High Flux, Xenocs, Sassenage, France) and $Cu_{K\alpha}$ radiation for **2**. Crystals were cooled using a Cryostream 800 open flow nitrogen cryostat (Oxford Cryosystems).

Data collection and image processing was performed with X-Area 1.75 [27]. Intensity data were scaled with LANA (part of X-Area) in order to minimize differences of intensities of symmetry-equivalent reflections. The structures were solved using intrinsic phasing procedure implemented in SHELXT and all non-hydrogen atoms were refined with anisotropic displacement parameters by full-matrix least squares procedure based on F2 using the SHELX–2014 program package [28,29]. The Olex2 [30] and Wingx [31] program suites were used to prepare the final version of CIF files. Olex2 [30] and Mercury [32] were used to prepare the figures.

Hydrogen atoms were refined using isotropic model with Uiso(H) values fixed to be 1.2 or 1.5 times U_{eq} of the carbon atoms to which they were attached. Hydrogen atoms bonded to the electronegative oxygen or nitrogen atoms were located in the electron density maps and refined without constraints. In the crystal structure of **4**, one of the *o*-vanillinate residues was modelled as disordered over two positions with SIMU restraints on all atoms. The atoms that belong to solvating methanol in **4** were refined with free occupancy factors, which converged approx. to 0.5.

To obtain a better starting model of **1** for the DFT calculations the aspherical refinement was performed in Olex2 [30]. The aspherical scattering factors were determined by NoSpherA2 [33] based on the wave function calculated in Orca5 [34,35] at the PBE/cc-pVTZ level of theory. H atoms were allowed to move freely (no AFIXs were used), and the ellipsoids were also refined. However, some RIGU constraints were needed because several H-atom ellipsoids were flattened or elongated. We note here that after the aspherical refinement, R1 dropped from 4.88 (independent atom model; spherical scattering factors) to 4.23 (Hirshfeld atom refinement; aspherical scattering factors). The table with the aspherical refinement data is included in the Supporting materials (Table S3).

2.4. NMR spectrometry and FT-IR spectroscopy

1D (^1H, $^{13}C\{^1H\}$) and 2D NMR spectra of **1** were recorded on a Bruker AV400 MHz spectrometer (external standard TMS for ^1H and ^{13}C) at ambient temperature. Equilibrium shift from aminal side to imine side was monitored by variable-temperature (VT) ^1H NMR of 0.005 g **1** (0.015 mmol) in DMSO-d_6 (0.7 mL). Data were processed using Bruker's Topspin 3.5 software. Symbols of atoms of **1** in the NMR spectrum were assigned according to the labels given in the X-ray crystal structure. Moreover, ^1H NMR chemical shifts for **1** and Schiff base: 2-methoxy-6-(2-pyrimidyliminomethyl)-phenol **1a** were predicted using free trial of MestReNova 14 software.

FT-IR spectrum of **1** was recorded for the crystalline product using Nicolet iS50 equipped with Specac Quest diamond ATR device; the spectrum was collected and formatted by OMNIC software. The FT-IR band assignments of **1** are presented in Supplementary materials (part S3).

2.5. DFT calculations

The initial structures of the *o*-vanillin imines derived from (2,3,4)-aminopyridine, 2-aminopyrimidine, and 2-amino-1,3,5-triazine were hand-drawn in GaussView 6.1 [36] and preoptimized. Then the *in vacuo* optimizations were performed at the B3LYP/6-311++G(d,p) level of theory incorporating Grimme's D3 dispersion correction in Gaussian 16 rev. C.01 [37]. After optimization, vibrational analyses were performed to ensure that the structures are within a local minimum of the potential energy surface (there were no negative frequencies in each case). Finally, the canonical orbitals were localized via the NBO procedure [38] implemented in Gaussian 16.

Subsequent orbital and electron density analyses were performed using Multiwfn 3.8 [39]. To examine the potential reactivity of the compounds studied, a bunch of parameters was calculated for the C═N bonds of imines. These include:

- d, Å – the bond length
- $\int \delta g^{pair}\ \mathbf{dr}$ – the integral over the difference between gradients for pairs of independent and bonded atoms [40]
- $IBSI^{IGMH}$ – the intrinsic bond strength index defined in the framework of independent gradient model based on Hirshfeld partition of molecular density [41]
- BO^{Fuzzy} – the Fuzzy bond order for C═N [42]
- BO^{NBO} – the bond order calculated as half of the difference in the occupation of bonding and anti-bonding orbitals that participates in the formation of the C═N bond calculated by the NBO procedure [38]
- ρ_{BCP}, e – the electron density at the critical point of the C═N bond calculated according to the QTAIM methodology [43]

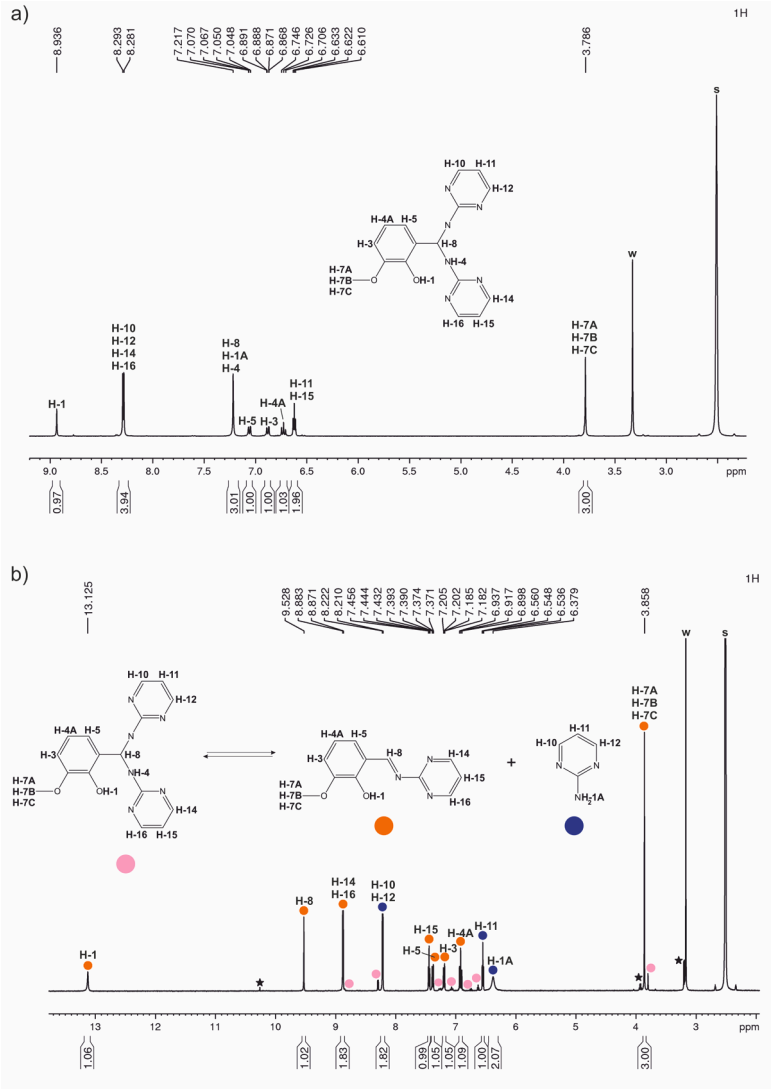

Fig. 1. ^{1}H NMR spectra (DMSO-d_6, 400 MHz) of: a) aminal **1** – spectrum obtained immediately after dissolution at RT; b) equilibrium of **1**/(**1a** + **AMP**) –NMR spectrum obtained for the sample thermostated at 333 K for 150 min.

- f^+, e – the value of the Fukui function f^+ reflecting susceptibility to nucleophilic attack on the imidic carbon atom [44]
- Δf, e – the dual descriptor indicating whether the imidic carbon atom is susceptible to nucleophilic attacks (more positive values) or electrophilic attacks (more negative values). [45].

The wavefunctions for ionized molecules necessary for calculation of the Fukui function and dual descriptor were obtained as single-point tasks in Gaussian 16 at the same level of theory as for optimization.

To assign the vibrations responsible for the occurrence of IR bands, we calculated the IR spectrum of aminal using the B3LYP/6-31+G(d,p) method with Grimme's D3 dispersion correction in Gaussian 16 rev. C.01 [37]. Although the IR frequencies had previously been calculated for an isolated aminal molecule, we aimed to account for the interactions present in the solid state. We extracted a pair of molecules and a trimer containing hydrogen bonds from the aspherically refined structure without further optimization. The hydrogen atoms were kept in their experimentally determined positions. Calculations for a system of three molecules proved too complex for the available computational resources, but calculations for a pair of molecules were successful. The obtained signal positions in cm^{-1} were linearly scaled as follows:

- in the range of 400–2000 cm^{-1}: $\tilde{\nu}_{sc} = 1.3 \times \tilde{\nu}_{calc} - 580$ [cm^{-1}]
- in the range of 2000–4000 cm^{-1}: $\tilde{\nu}_{sc} = 1.1 \times \tilde{\nu}_{calc} - 760$ [cm^{-1}]

In a subsequent attempt, we calculated the IR spectrum using periodic boundary conditions, which account for all interactions present in the solid-state structure. The calculations were performed using the CASTEP program (BIOVIA Materials Studio) [46] at the GGA/BLYP level of theory with Grimme's dispersion correction. The geometry was optimized with medium convergence requirements. In this case, scaling was not performed.

3. Results and discussion

3.1. Syntheses and NMR spectroscopy

The solutions of *o*-vanillin (OV) and 2-aminopyrimidine (2AMP) in different solvents were studied. It was observed that the mixture exhibits different colours in different temperatures indicating the temperature dependence of the equilibrium reaction undergoing between OV and 2AMP. The orange color in the elevated temperature in both MeOH and toluene suggested the formation of imine – imines with aromatic substituents at the imine bond are often orange or red-orange. In lower temperatures the solution of OV and 2AMP was yellow and produced colorless **1** as a single crystalline product. NMR spectroscopic studies

Table 2
^{1}H NMR chemical parameters (chemical shifts in ppm, multiplicity and coupling constants in Hz, DMSO-d_6, 400 MHz) for aminal **1**, Schiff base: 2-methoxy-6-(2-pyrimidyliminomethyl)-phenol **1a**, and 2-aminopyrimidine **2AMP**. See Fig. 1 for atom labeling.

Proton labels	Compounds					
	1		1a		2AMP	
	Multiplicity	δ [ppm]	Multiplicity	δ [ppm]	Multiplicity	δ [ppm]
OH-1	s	8.94	s	13.13		
CH-10	d (J = 4.8 Hz)	8.29	–		d (J = 4.8 Hz)	8.22
CH-12						
CH-14			d (J = 4.8 Hz)	8.88	–	
CH-16						
NH-1A	s	7.22	–		br s	6.38
NH-4						
CH-8			s	9.53	–	
CH-5	dd (J = 7.9, 1.2 Hz)	7.06	dd (J = 7.9, 1.2 Hz)	7.38		
CH-3	dd (J = 7.9, 1.2 Hz)	6.88	dd (J = 7.9, 1.2 Hz)	7.19		
CH-4A	t (J = 7.9 Hz)	6.73	t (J = 7.9 Hz)	6.92		
CH-11	t (J = 4.8 Hz)	6.62			t (J = 4.8 Hz)	6.55
CH-15			t (J = 4.8 Hz)	7.44	–	
CH-7A	s	3.79	s	3.86		
CH-7B						
CH-7C						

were consistent with the X-ray diffraction results and revealed the formation of an adduct of the imine and 2-aminopyrimidine *i.e.* aminal **1** (Scheme 1). The ^{1}H NMR spectrum of **1** shows set of signals for aminopyrimidine and *o*-vanillin rings with the singlet of OH group at 8.94 ppm (Fig. 1a, Table 2, Figures S1 – S9). A signal corresponding to methine (-CH-) group observed at 7.22 ppm overlaps with the signals of aminopyrimidine NH protons.

Variable-temperature (VT) ^{1}H NMR spectra recorded from 298 K to 333 K reflected dynamic properties of obtained heterocyclic amino aminal **1** and the aminal/imine exchange in solution (Scheme 1, Fig. 1b, Figure S8). A state of equilibrium with the molar ratio 8/92 for **1**/**1a** was reached at 333 K after 150 min of thermostating of the sample at this temperature. The ratio was determined by integration of well-separated signals of CH_3-O groups of *o*-vanillin rings in **1** and **1a** in the ^{1}H spectrum (Figure S7). Lowering the temperature to RT did not change the ratio of these two compounds. Comparable equilibrium with molar ratio 10/90 for **1**/**1a** is established seven days after dissolution of the aminal **1** in DMSO-d_6 at RT.

In-depth analysis of the obtained ^{1}H NMR spectra allowed unambiguous assignment of all proton signals of all compounds occurring in solution (Fig. 1, Table 2, Figure S7), confirming the above-described equilibrium. Signal of -C***H***=N- proton in **1a** occurred at 9.53 ppm in the range typical for the imine carbon [2,3] (Fig. 1b). Moreover, broad signal of OH group in **1a** exhibited a chemical shift characteristic for enol/imine form of this compound 13.13 ppm [2].

The predicted ^{1}H NMR spectra for **1** and **1a** confirmed the chemical shifts assignment (Figure S9 and S10). The largest differences in shift values were observed for protons bonded to heteroatoms (OH and NH) in the analyzed compounds and the proton of the methine group (Table S1 and S2).

In Scheme 2 we summarize our earlier findings regarding the reactions of *o*-vanilline and aminopyridine isomers [2] and the present result. Previously we managed to synthesize the reactive imine **C** in carefully dried toluene. Now we have attempted to isolate imine **1a** by reaction of OV and 2AMP in toluene, subsequent removal of the toluene by distillation and drying the orange residue to prevent the formation of amine (as a result of hydrolysis of imine). However, after dissolution of the residue in any solvent for recrystallization we obtained colorless aminal **1** as the only solid product.

Another attempt to force the formation of imine was the addition of various metal salts to the solution of OV and 2AMP. Since our ultimate goal is the synthesis of metal - imine complexes we tried to investigate whether metal ions could have the templating effect and form such complexes in the presence of OV and 2AMP. Though we observed that the addition of zinc(II) and cadmium acetates with the subsequent warming resulted in the change of color of the reaction mixtures from yellow to orange, we have not been able to isolate the complexes of imine **1a** in the crystalline form. The products of the reactions between metal acetates, OV and 2AMP are shown in Scheme 3 and further described in the following chapter 4.2.

3.2. Crystal structures

The crystal structure of aminal **1** is presented in the Fig. 2. Compound **1** crystallizes as well-formed, colorless crystals from methanol/ethanol and toluene solutions of OV and 2AMP. The asymmetric unit

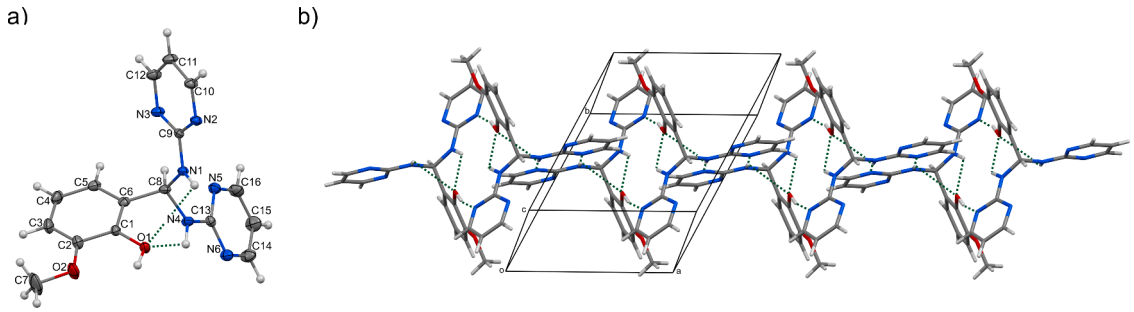

Fig. 2. Crystal structure of **1**, H-bonds indicated with the green dashed lines: a) molecular structure with the numbering scheme, displacement ellipsoids drawn at the 30% probability level, important bond lengths [Å]: O1−C1 1.366(3), C6−C8 1.517(3), N1−C8, 1.459(3), N4−C8 1.438(3); b) view of the unit cell and the hydrogen-bonded chain.

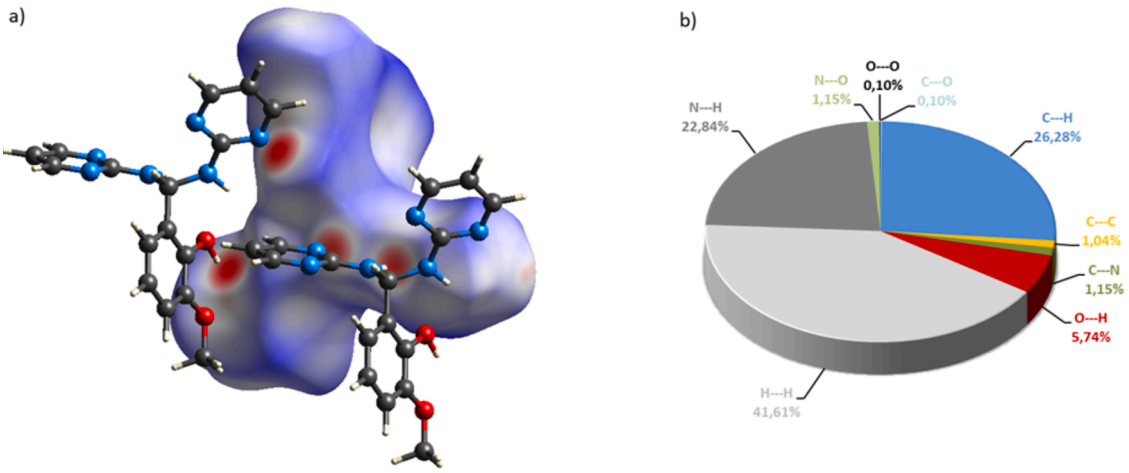

Fig. 3. a) Hirshfeld surfaces of **1**. Red color: normalized contact distances d_{norm} shorter than the sum of van der Waals radii (d_{norm}= −0.630), white color: van der Waals contacts (d_{norm}= 0.517), and blue color: normalized contact distances exceeding the sum of van der Waals radii (d_{norm}= 1.718); b) Hirshfeld surface fingerprint decompositions showing the main types of interactions for **1**.

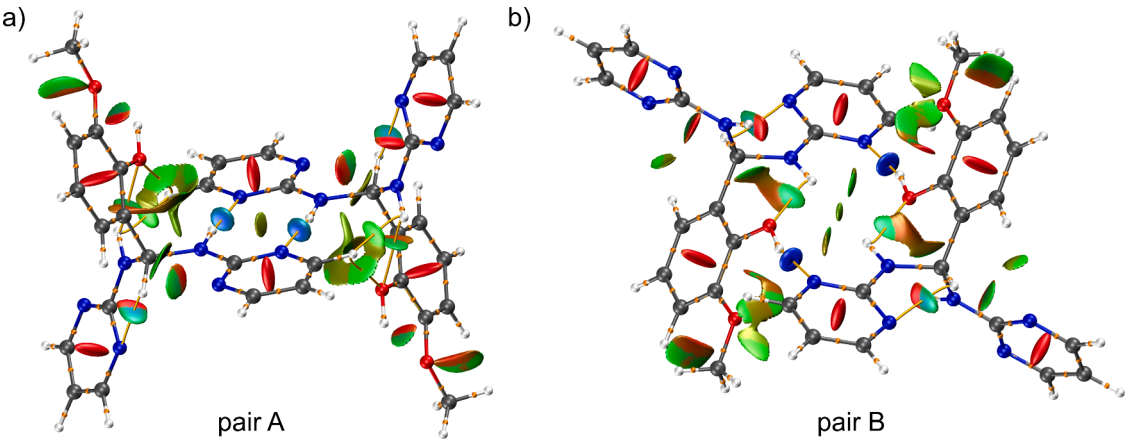

Fig. 4. Visualization of the NCI analysis for the two types of hydrogen bonded pairs in the crystal structure of **1**. Red surfaces designate strong repulsions, green surfaces are the weak van der Waals interactions, and blue surfaces are the strong attractive interactions. The orange points are the QTAIM's bond critical points. Graphics was prepared using VMD [48].

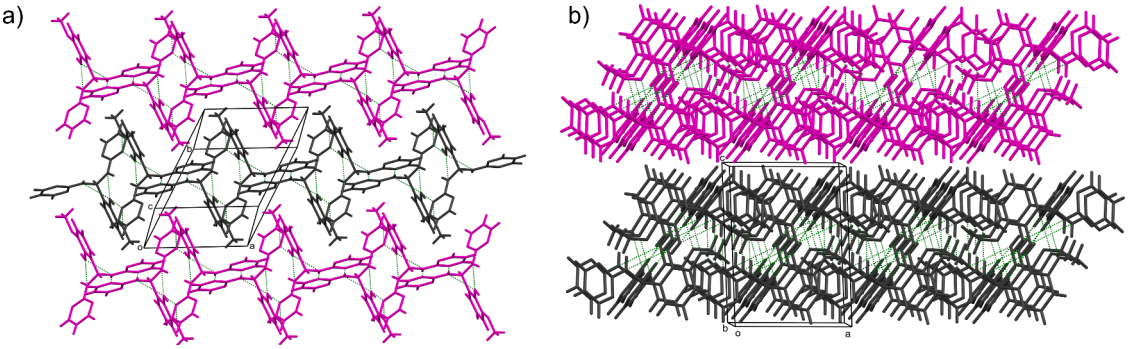

Fig. 5. Crystal packing of **1**, hydrogen bonds indicated with the green dashed lines: a) arrangement of molecules within a layer; b) ordering of layers.

contains the whole molecule therefore we can observe small differences between the C-N bond lengths of the aminal functional group (see Fig. 2 caption). The crystal structure of **1** was also solved with the aspherical crystal structure refinement to obtain a better starting model for DFT calculations. The obtained data are presented in Supplementary materials as Table S3 and Fig. S12.

The crystal packing that results from the intermolecular interactions is illustrated in Fig. 2b, Fig. 3a and b, Fig. 4a and b, Fig. 5a and b. The classical hydrogen bonds O–H···N and N–H···N assemble the molecules of the aminal into the H-bonded chains propagating along the *a*-axis of the unit cell (Fig. 2b). In Fig. 3 these relatively strong interactions are shown as four red spots *i.e.* short contacts at Hirshfeld surfaces. The red areas on the Hirshfeld surface correspond to strong interactions between $O1_{[-x+1,-y+1,-z+1]}$−H···N2, O1−H···$N6_{[-x+1,-y+1,-z+1]}$, N1−H···$N2_{[-x,-y+1,-}$

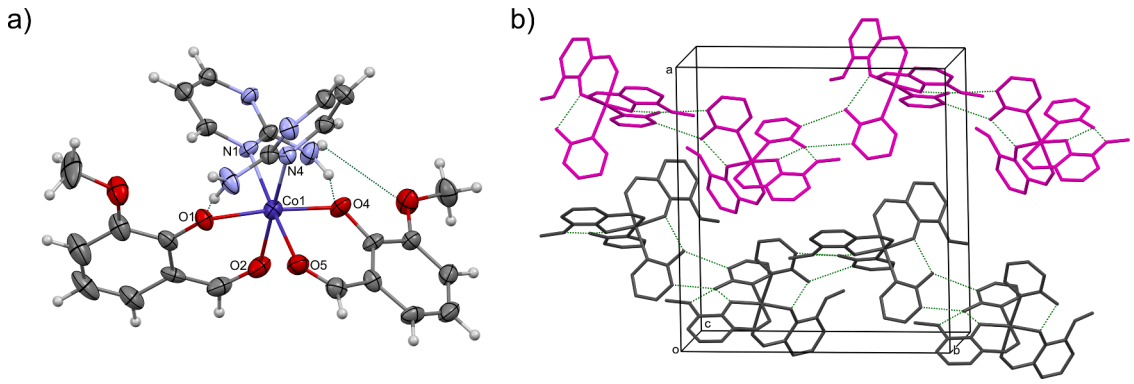

Fig. 6. Crystal structure of **2**: a) molecular structure with the heteroatoms numbering scheme, displacement ellipsoids drawn at the 50% probability level, important bond lengths [Å]: Co1−O1 2.004(5), Co1−O2 2.140(5), Co1−O4, 1.992(5), Co1−O5 2.139(6), Co1−N1 2.234(6), Co1−N4 2.195(5); b) crystal packing with the cell axes and hydrogen bonds as green dashed lines.

$_{z+1]}$ and N1$_{[-x,-y+1,-z+1]}$−H···N2. The decomposed fingerprint plot shows that "outside" the chains the major factor in the crystal packing are the hydrophobic H···H (41.61%) interactions, with C···H (26.28%) representing the next highest contribution. The crystal packing resulting from these interactions will be further described in Fig. 5ab.

To analyze the intermolecular interactions present in the structure of **1**, the NCI analysis was also used [47]. Within the chains there are two types of pairs, which we denote A and B that are bonded interchangeably into the tight arrangement. These pairs are illustrated separately in Fig. 4a and b. Pair A incorporates only N1−H···N2$_{[-x,1-y,1-z]}$/N1$_{[-x,-y+1,-z+1]}$−H···N2 hydrogen bonds, while B uses N4−H···O1$_{[1-x,1-y,1-z]}$ and O1−H···N6$_{[1-x,1-y,1-z]}$. These hydrogen bonds are indicated as blue blobs. The steric effects of the rings are also visible (red blobs). The green patches are the regions of the less obvious weak interactions revealed by the NCI analysis.

In both pairs, intermolecular rings are formed with green blobs inside that indicate an attractive interaction. Furthermore, the weak H-bonds C10−H···O1$_{[-1+x,y,z]}$ and tentatively N4−H···H−C10$_{[-x,1-y,1-z]}$, so-called hydrogen-hydrogen bonds interactions are visible in A [49]. Within the pair B illustrated in Fig. 4b, a more complex pattern is present. Two smaller S(6) rings are incorporated into the large $R_4^4(12)$ ring [50]. Small rings are formed by means of weak intramolecular N4−H···O1 hydrogen bonds with N−H···O angle of 117° The N4−H···O1 hydrogen bond is revealed only by NCI while there is no QTAIM bond path. The N4−H···H−N4$_{[1-x,\ 1-y,\ 1-z]}$ hydrogen-hydrogen bond may be additionally considered.

Finally in Fig. 5a and b we illustrate the mutual arrangement of chains and layers of **1**. The chains are quite tightly packed into 2-D arrangement in the crystallographic *ab* plane *via* some directional contacts such as C−H···π and C−H···N *e.g.* C14−H ··C4$_{[x,1+y,z]}$ 3.593(5) Å and C15−H ··N3$_{[x,1+y,z]}$ 3.569(4) Å. The interactions between the layers are only dispersive London forces. The ordering of chains and layers in crystals of **1** is illustrated in Fig. 5a and b. The multiple hydrogen bonding and CH···π/N interactions make an important contribution to the overall attractive forces; we suggest that they may constitute an important force, driving the ultimate crystallization of aminal instead of the imine from the equilibrium mixture.

The remaining crystal structures described in this section are the structures of complexes **2** – **4** that form in solutions containing metal ions (as acetates), 2-aminopyrimidine and *o*-vanillin. We have noted the formation of four coordination compounds in reactions of cobalt(II) and copper(II) salts whereas in the solutions of 2AMP and OV with zinc(II) and cadmium(II) acetates we only observed the formation of aminal **1**.

As showed in Fig. 6a compound **2** is an octahedral complex of Co(II) with two vanillinate and two 2AMP ligands. It was isolated as one of two possible isomers *i.e.* isomer *cis*. In the crystals the molecules of **2** interact *via* NH···O hydrogen bonds with the formation of folded layers as illustrated in Fig. 6b. Among the products of the reaction of Co(II) acetate with the OV and 2AMP in methanol we have also identified a known cubane **2a** by its unit cell parameters (Scheme 3) [26].

Complex **3** that was found among the products of the reaction of copper(II) acetate with OV and 2AMP is a 1-D coordination polymer that features two different coordination centers linked via 2AMP molecules. The particular crystal structure of copper(II) acetate, so called "Chinese lantern" or "paddle wheel" motif, is partly preserved in the polymer whereas the other bead in the chain is planar Cu(II) o-vanillinate (Fig. 7a). The three copper atoms, 2AMP ring and two of the four carboxylates forming the Chinese lantern motive lay in approximately one plane, whereas oxygen ligands *i.e.* vanillinate and two other carboxylates lay above and below this plane.

The compound **4** identified in the solution containing 2AMP, OV and Cu is a known vanillinate complex of Cu(II) [51,52]. It is a different solvate though and we present the molecular structure of the complex as Supplementary content (Fig. S13).

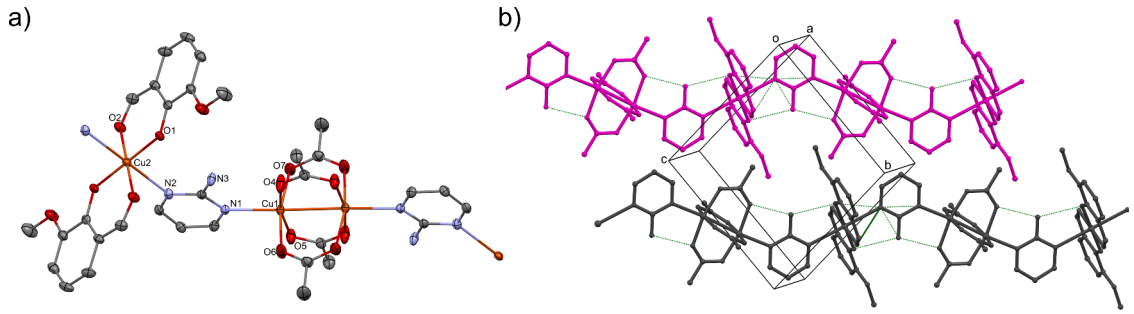

Fig. 7. Crystal structure of **3**: a) molecular structure with the heteroatoms numbering scheme, displacement ellipsoids drawn at the 50% probability level, important bond lengths [Å]: Cu1−N1 2.2285(16), Cu1−O4 1.9687(16), Cu1−O5$_{[-x,1-y,2-z]}$ 1.9735(15), Cu1−O6, 1.9592(16), Cu1−O7$_{[-x,1-y,2-z]}$ 1.9597(16), Cu2−N2 2.4774 (16), Cu2−O1 1.9137(13), Cu2−O2 1.9928(14); b) crystal packing with the cell axes and hydrogen bonds as green dashed lines.

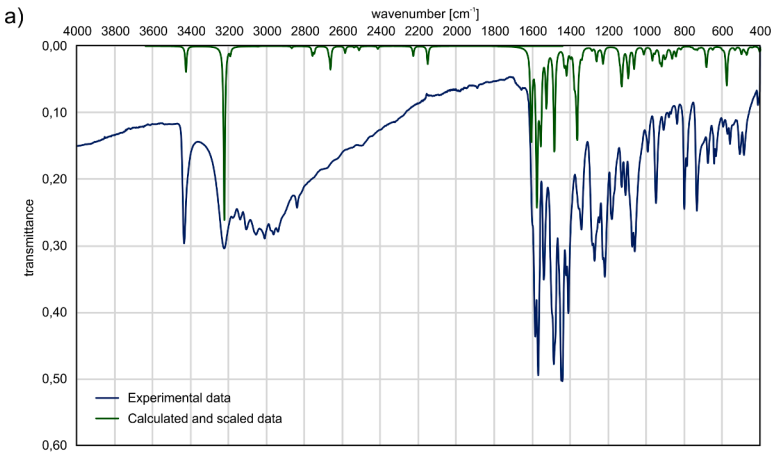

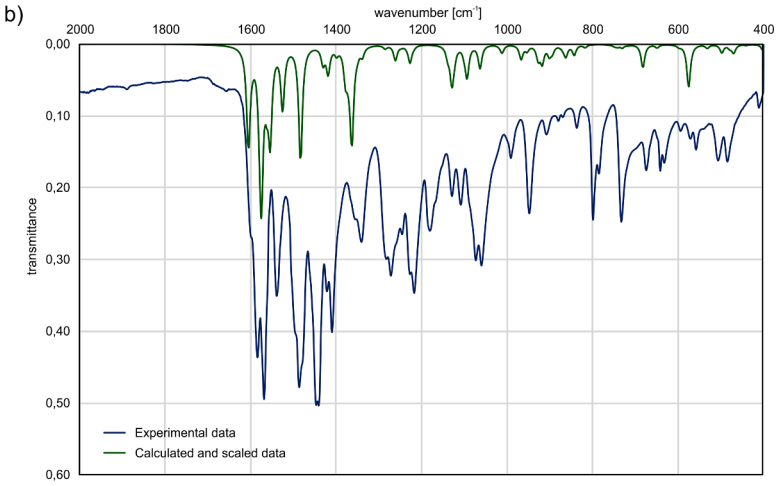

Fig. 8. The comparison of experimental (blue) and calculated at B3LYP/6-31+G(d,p) GD3 level of theory (green) IR spectra of **1** (pair A): a) the whole range 4000–400 cm^{-1}; b) the fingerprint region. In the whole range of the spectrum (400–4000 cm^{-1}) the intensities of the bands of the calculated spectrum have been multiplied by the factor $5{\cdot}10^{-5}$.to improve the readability of the figure: The obtained signal positions in cm^{-1} were linearly scaled: in the range of 400–2000 cm^{-1}: $\tilde{\nu}_{sc} = 1.3 \times \tilde{\nu}_{calc} - 580$ [cm^{-1}]; in the range of 2000–4000 cm^{-1}: $\tilde{\nu}_{sc} = 1.1 \times \tilde{\nu}_{calc} - 760$ [cm^{-1}].

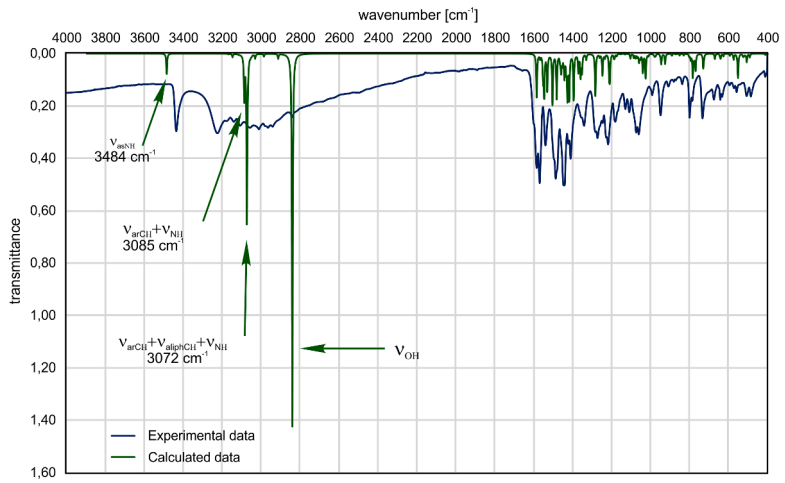

Fig. 9. The comparison of experimental (blue) and calculated in the periodic boundary conditions (green [46]) IR spectra of **1**. The green arrows point to the X-H stretching modes in the calculated spectrum.

3.3. FT-IR spectroscopy

The aminal **1** was characterized in solid state by ATR FT-IR spectroscopy. Moreover, the IR spectra were calculated by two approaches. Initially, we have applied DFT calculations at the B3LYP/6-311+G(d,p) D3 level (Gaussian 16 rev. C.01) to calculate the frequencies for the dimer of **1** (pair A, see Fig. 4 in 3.2). The calculated spectrum required scaling to reproduce the experimental data. After scaling, the differences between the experimental and calculated spectrum were observed mainly in the region 3600–2200 cm^{-1} (Fig. 8). The intense IR continua visible in this region of the experimental spectrum clearly indicate and confirm the presence of the hydrogen bonded chains in the solid state,

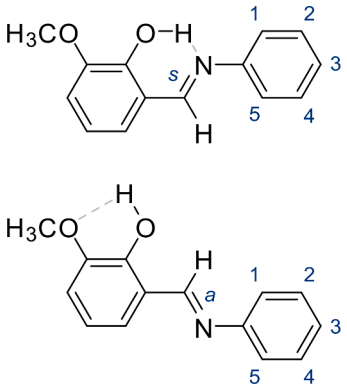

Nitrogen atoms at:

*s*1	*a*1
*s*2	*a*2
*s*3	*a*3
*s*4	*a*4
*s*5	*a*5
*s*15	*a*15
*s*135	*a*135

Scheme 4. Symbols of the optimized molecules/geometries.

which are not reflected in the calculated spectrum. The systems containing polarizable protons, protons-conducting systems or systems with the excess protons are known to generate similar continua as studied in several papers of Zundel and other authors [53–57]. Other inconsistencies may result from the simplicity of the system – the calculations were performed for the fragment of the chain and the FT-IR ATR spectra were measured for the crystalline material (*quasi*-infinite system).

We then decided that the periodical calculations would return a more accurate picture of the FT-IR ATR spectrum. The periodic boundary conditions were simulated using the CASTEP program at the GGA/BLYP level of theory. As illustrated in Fig. 9, in this case the fingerprint region was reproduced correctly without scaling. Although the X-H stretching modes were localized at a well-defined wavenumber, which does not correspond to the experimental spectrum (Fig. 9), their energies were, in our opinion, correctly assigned. We would like to point to the relatively low wavenumber of OH stretching mode in the spectrum calculated in the periodic conditions. In our opinion it accurately reflects the acidic character of the phenolic hydrogen, which is additionally engaged in the chain of the hydrogen bonds (Fig. 9). Moreover, the calculations depict the situation at 0 K, while the spectrum was measured at RT.

Most of the bands observed in the FT-IR spectrum are complex modes of the aminal molecule. We have undertaken the effort to describe them in Tables S4 (pair A, Gaussian) and Table S5 (periodical system, CASTEP) of Supplementary materials. Once more we would like to recommend the assignments that resulted from periodical calculations.

3.4. DFT calculations

To examine the influence of nitrogen substituents on the potential reactivity of selected imines, two sets of geometries were studied by theoretical methods – one with imine N-atom close to OH group (conformation ***s***) and the other where it is distant (conformation ***a***). In each series compounds with one, two, or three CH groups substituted with N-atom were prepared. The single substitution was rationalized in five different positions: two *ortho*, two *meta*, and one *para* (Scheme 4).

As is known from our previous study, while *o*-vanillin reacts with 4-aminopyridine in methanol, the α-aminoether is formed which is not observed for other aminopyridines [2]. This proved that compound *s*3 (Scheme 4) is most susceptible for nucleophilic attack. Also compound *s*15, that we have tried to isolate within this study, is susceptible for this kind of reaction but rather with another molecule of amine than solvent molecule. For this reason, *s*3 and *s*15 are considered the most reactive. We have calculated a set of parameters (Table 4) to check how they correlate with the reactivity. Considering the bond length (*d*), it should be expected that the longer it is, the more reactive the compound will be. However, we do not observe such a relation (*s*3 is excluded from the otherwise visible correlation). The following parameters measure the bond strength ($\int \delta g^{pair}$ dr, $IBSI^{IGMH}$), the bond order (BO^{Fuzzy}, BO^{NBO}), and the electron density (ρ_{BCP}) and are expected to be the lowest for *s*3 and *s*15, yet again this is not the case. However, it must be noted that bond orders are relatively low for both *s*15 and *s*135. Fukui f^+ function should be the largest for these two compounds as the C=N bond is most

Table 4
Selected parameters for C=N bonds derived from DFT-optimized structures. The symbols are described in the experimental part. Table cells are colored in such a way that the largest numerical values in a given column/conformation ***s/a*** are dark green and the smallest value(s) are light green.

Code	*d*, Å	$\int \delta g^{pair}$ dr	$IBSI^{IGMH}$	BO^{Fuzzy}	BO^{NBO}	ρ_{BCP}, e	f^+, e	Δf, e
*s*1	1.2874	0.5825	0.7018	1.9097	1.8350	0.3612	0.1071	0.0970
*s*2	1.2894	0.5834	0.7007	1.9091	1.8360	0.3592	0.1069	0.0956
*s*3	1.2897	0.5823	0.6991	1.9065	1.8343	0.3595	0.1083	0.1006
*s*4	1.2899	0.5831	0.6998	1.9074	1.8367	0.3589	0.1078	0.0975
*s*5	1.2941	0.5880	0.7011	1.8919	1.8332	0.3572	0.1053	0.0954
*s*15	1.2953	0.5864	0.6979	1.8858	1.8288	0.3575	0.1079	0.0998
*s*135	1.2995	0.5837	0.6902	1.8756	1.8210	0.3557	0.1096	0.1002
*a*1	1.2827	0.5959	0.7231	1.9215	1.8644	0.3668	0.0998	0.0732
*a*2	1.2802	0.5913	0.7204	1.9320	1.8668	0.3675	0.1001	0.0719
*a*3	1.2794	0.5893	0.7190	1.9318	1.8655	0.3683	0.1024	0.0804
*a*4	1.2796	0.5911	0.7208	1.9338	1.8667	0.3678	0.0999	0.0699
*a*5	1.2771	0.5873	0.7191	1.9344	1.8660	0.3700	0.1007	0.0754
*a*15	1.2808	0.5931	0.7220	1.9191	1.8615	0.3689	0.1041	0.0892
*a*135	1.2827	0.5905	0.7167	1.9129	1.8555	0.3680	0.1079	0.1031

susceptible to nucleophilic attack; it is observed – however we would expect lower value for *s*4. Finally, in the case of the last parameter *i.e.* dual descriptor (Δf), we observe the expected relation. The largest numerical values correspond to the most reactive compounds, while the smaller numerical values represent the compounds that are easily isolable (less reactive). The accuracy of the dual descriptor for measuring local reactivity was previously discussed in [58]. Moreover, the high value of *d*, f^+ and Δf for compound s/a135 indicates that this compound should be also reactive – and therefore avoided as a potential building block for the construction of imines as potential ligands.

4. Conclusions

As we observed for the reactions of *o*-vanillin and aminopyridines/aminopyrimidine, the imines derived from heterocyclic nitrogen compounds are often reactive species that relatively easily undergo nucleophilic addition. Previously, we proved it for imine derived from 4-aminopyridine and now we confirm it for the derivative of 2-aminopyrimidine. Interestingly, depending on the solvent, and solubility of the possible products of addition, the reaction between the newly formed imine and other participants of the reaction mixture may be directed toward different products: hemiaminal ether [2] or aminal [3, this work]. We confirmed that the dual descriptor is the most suitable parameter for testing the reactivity of the newly synthesized imines to exclude potentially very reactive species that are difficult to isolate [58].

CRediT authorship contribution statement

Magdalena Siedzielnik: Conceptualization, Synthetic experiments, Writing – original draft, Writing – review & editing. **Andrzej Okuniewski:** DFT calculations, Writing – original draft. **Kinga Kaniewska-Laskowska:** NMR experiments, Writing – original draft, Writing – review & editing. , **Marcin Erdanowski:** Synthesis of a cobalt(II) complexes. **Anna Dołęga:** Conceptualization, Validation, Supervision, Funding acquisition, XRD experiments, Structure solution, Writing – original draft, Writing – review & editing.

Declaration of Competing Interest

The authors declare that they have no known competing financial interests or personal relationships that could have appeared to influence the work reported in this paper.

Data availability

Data will be made available on request.

Acknowledgment

The research was supported by the "Excellence Initiative - Research University" program at Gdańsk University of Technology SILICIUM SUPPORTING CORE R&D FACILITIES DEC-2/2021/IDUB/V.6/Si.

Supplementary materials

Supplementary material associated with this article can be found, in the online version, at doi:10.1016/j.molstruc.2023.135847.

References

[1] S.E. Denmark, N. Nakajima, O.J.-C. Nicaise, Asymmetric addition of organolithium reagents to imines, J. Am. Chem. Soc. 116 (1994) 8797–8798, https://doi.org/10.1021/ja00098a044.
[2] A. Mielcarek, A. Wiśniewska, A. Dołęga, Unassisted formation of hemiaminal ether from 4-aminopyridine and o-vanillin - experimental and theoretical study, Struct. Chem. 29 (2018) 1189–1200, https://doi.org/10.1007/s11224-018-1105-5.
[3] J.-M. Ciou, H.-F. Zhu, C.-W. Chang, J.-Y. Chen, Y.-F. Lin, Physical organic studies and dynamic covalent chemistry of picolyl heterocyclic amino aminals, RSC Adv. 10 (2020) 40421–40427, https://doi.org/10.1039/D0RA08527H.
[4] G.R. Heintzelman, I.R. Meigh, Y.R. Mahajan, S.M. Weinreb, Diels-alder reactions of imino dienophiles, Org. React. 65 (2005) 141–599, https://doi.org/10.1002/0471264180.or065.02.
[5] T.T. Tidwell, Hugo (Ugo) Schiff, Schiff bases, and a century of beta-lactam synthesis, Angew. Chem. Int. Ed. 47 (2008) 1016–1020, https://doi.org/10.1002/anie.200702965.
[6] A. Milenkovic, F. Fache, R. Faure, M. Lemaire, Activated imines and aminal derivatives: potential precursors of β-amino acids, Synth. Commun. 29 (1999) 1535–1546, https://doi.org/10.1080/00397919908086133.
[7] F. Chang, D. Zhang, G. Xu, H. Yang, J. Li, H. Song, W.-H. Sun, Synthesis and characterization of new bis(1-aryliminomethylenylnaphthalen-2-oxy)nickel complexes and their catalytic behavior for vinyl polymerization of norbornene, J. Organomet. Chem. 689 (2004) 936–946, https://doi.org/10.1016/j.jorganchem.2003.12.024.
[8] W.-G. Jia, H. Zhang, T. Zhang, D. Xie, S. Ling, E.-H. Sheng, Half-sandwich ruthenium complexes with schiff-base ligands: syntheses, characterization, and catalytic activities for the reduction of nitroarenes, Organometallics 35 (2016) 503–512, https://doi.org/10.1021/acs.organomet.5b00933.
[9] S.-D. Su, J.-X. Li, F. Xu, C.-X. Wang, K. Wang, Y. Li, S.-H. Zhang, X.-Q. Zhang, Y.-Q. Zhang, F.P. Liang, Dy^{III} single-molecule magnets from ligands incorporating both amine and acylhydrazine Schiff base groups: the centrosymmetric $\{Dy_2\}$ displaying dual magnetic relaxation behaviors, Dalton Trans. 49 (2020) 15739–15749, https://doi.org/10.1039/C9DT04434E.
[10] B. Cristóvão, D. Osypiuk, B. Miroslaw, A. Bartyzel, Heterometallic di- and trinuclear $Cu^{II}Ln^{III}$ (Ln^{III} = La, Ce, Pr, Nd) complexes with an alcohol-functionalized compartmental Schiff base ligand: Syntheses, crystal structures, thermal and magnetic studies, Polyhedron 188 (2020), 114703, https://doi.org/10.1016/j.poly.2020.114703.
[11] M. Barwiolek, D. Jankowska, M. Chorobinski, A Kaczmarek-Kędziera, I. Łakomska, S. Wojtulewski, T.M. Muzioł, New dinuclear zinc(ii) complexes with Schiff bases obtained from o-phenylenediamine and their application as fluorescent materials in spin coating deposition, RSC Adv. 11 (2021) 24515–24525, https://doi.org/10.1039/D1RA03096E.
[12] X. Lei, Y. Zou, Q. Liang, W. Xu, S. Lao, B. Yang, L. Li, L. Yang, H. Liu, L.-J. Ma, An ultrasensitive 4-(Diethylamino) salicylaldehyd-based fluorescence enhancement probe for the detection of Al^{3+} in aqueous solutions and its application in cells, J. Photochem. Photobiol. A: Chem. 428 (2022), 113854, https://doi.org/10.1016/j.jphotochem.2022.113854.
[13] C.M. Fernandes, V.G.S.S. Pina, C.G. Alfaro, M.T.G. de Sampaio, F.F. Massante, L. X. Alvarez, A.M. Barrios, J.C.M. Silva, O.C. Alves, M. Briganti, F. Totti, E.A. Ponzio, Innovative characterization of original green vanillin-derived Schiff bases as corrosion inhibitors by a synergic approach based on electrochemistry, microstructure, and computational analyses, Colloids Surf. A 641 (2022), 128540, https://doi.org/10.1016/j.colsurfa.2022.128540.
[14] B. Cristóvão, D. Osypiuk, A. Bartyzel, New Heterotrinuclear $Cu^{II}Ln^{III}Cu^{II}$ (Ln = Ho, Er) Compounds with the Schiff Base: Syntheses, Structural Characterization, Thermal and Magnetic Properties, Materials 15 (2022) 4299, https://doi.org/10.3390/ma15124299.
[15] C.M. da Silva, D.L. da Silva, L.V. Modolo, R.B. Alves, M.A. Resende, C.V.B. Martins, A. de Fatima, Schiff bases: A short review of their antimicrobial activities, J. Adv. Res. 2 (2011) 1–8, https://doi.org/10.1016/j.jare.2010.05.004.
[16] M.T. Kaczmarek, M. Zabiszak, M. Nowak, R. Jastrząb, Lanthanides: Schiff base complexes, applications in cancer diagnosis, therapy, and antibacterial activity, Coord. Chem. Rev. 370 (2018) 42–54, https://doi.org/10.1016/J.CCR.2018.05.012.
[17] Y. Qin, P. Li, Antimicrobial chitosan conjugates: current synthetic strategies and potential applications, Int. J. Mol. Sci. 21 (2020) 499, https://doi.org/10.3390/ijms21020499.
[18] R. Pis-Diez, G.A. Echeverría, O.E. Piro, J.L. Jios, B.S. Parajón-Costa, A structural, spectroscopic and theoretical study of an o-vanillin Schiff base derivative involved in enol-imine and keto-amine tautomerism, New J. Chem. 40 (2016) 2730–2740, https://doi.org/10.1039/c5nj01039j.
[19] A.M. Dąbrowska, P. Mech-Warda, M. Wera, M. Domżalska, M. Makowski, A. Chylewska, Prototropic tautomerism of (E)-N-((4-((2-hydroxy-5-methoxybenzylidene) amino)phenyl)-sulfonyl)acetamide and its coordination abilities towards Ru, Rh, and Ir trivalent metal ions, Polyhedron 222 (2022), 115909, https://doi.org/10.1016/j.poly.2022.115909.
[20] A. Hameed, M. al-Rashida, M. Uroos, S.A. Ali, K.M. Khan, Schiff bases in medicinal chemistry: a patent review (2010-2015), Expert Opin. Ther. Pat. 27 (2017) 63–79, https://doi.org/10.1080/13543776.2017.1252752.
[21] C. Giri, F. Topić, P. Mal, K. Rissanen, Anion-controlled formation of an aminal-(bis) imine Fe(II)-complex, Dalton Trans. 43 (2014) 15697–15699, https://doi.org/10.1039/C4DT02180K.
[22] G. Ahmad, N. Rasool, K. Rizwan, A.A. Altaf, U. Rashid, M.Z. Hussein, T. Mahmood, K. Ayub, Role of pyridine nitrogen in palladium-catalyzed imine hydrolysis: a case study of (E)-1-(3-bromothiophen-2-yl)-N-(4-methylpyridin-2-yl)methanimine, Molecules 24 (2019) 2609, https://doi.org/10.3390/molecules24142609.
[23] A. Mielcarek, A. Bieńko, P. Saramak, J. Jezierska, A. Dołęga, A Cu/Zn heterometallic complex with solvent-binding cavity, catalytic activity for the oxidation of 1-phenylethanol and unusual magnetic properties, Dalton Trans. 48 (2019) 17780–17791, https://doi.org/10.1039/C9DT03304A.

[24] M. Siedzielnik, D.A. Pantazis, K. Kaniewska-Laskowska, J. Bruniecki, A. Dołęga, The reactivity of the imine bond within polynuclear nickel(II) complexes, Crystals 11 (2021) 512, https://doi.org/10.3390/cryst11050512.
[25] M. Siedzielnik, M. Pawłowska, M. Daśko, H. Kleinschmidt, A. Dołęga, Reactions of cobalt(II) chloride and cobalt(II) acetate with hemisalen-type ligands: ligand transformation, oxidation of cobalt and complex formation. Preliminary study on the cytotoxicity of Co(II) and Co(III) hemisalen complexes, RSC Adv. 13 (2023) 8830–8843, https://doi.org/10.1039/D2RA07089H.
[26] S.-H. Zhang, Y. Song, H. Liang, M.-H. Zeng, Microwave-assisted synthesis, crystal structure and properties of a disc-like heptanuclear Co(II) cluster and a heterometallic cubanic Co(II) cluster, CrystEngComm 11 (2009) 865–872, https://doi.org/10.1039/B815675A.
[27] X-Area 1.75, STOE & Cie GmbH, Software Package for Collecting Single-Crystal Data on STOE Area-Detector Diffractometers, for Image Processing, Scaling Reflection Intensities and for Outlier Rejection, STOE, Darmstadt, Germany, 2015.
[28] G.M. Sheldrick, SHELXL-2014, University of Göttingen and Bruker AXS, Karlsruhe, Germany, 2014.
[29] G.M. Sheldrick, Crystal structure refinement with SHELXL, Acta Crystallogr. C 71 (2015) 3–8, https://doi.org/10.1107/S2053229614024218.
[30] O.V. Dolomanov, L.J. Bourhis, R.J. Gildea, J.A.K. Howard, H.J. Puschmann, OLEX2: a complete structure solution, refinement and analysis program, J. Appl. Crystallogr. 42 (2009) 339–341, https://doi.org/10.1107/S0021889808042726.
[31] L.J. Farrugia, WinGX and ORTEP for windows: an update, J. Appl. Crystallogr. 45 (2012) 849–854, https://doi.org/10.1107/S0021889812029111.
[32] C.F. Macrae, P.R. Edgington, P. McCabe, E. Pidcock, G.P. Shields, R. Taylor, M. Towler, J. van de Streek, Mercury: visualization and analysis of crystal structures, J. Appl. Crystallogr. 39 (2006) 453–457, https://doi.org/10.1107/S002188980600731X.
[33] F. Kleemiss, O.V. Dolomanov, M. Bodensteiner, N. Peyerimhoff, L. Midgley, L. J. Bourhis, A. Genoni, L.A. Malaspina, D. Jayatilaka, J.L. Spencer, F. White, B. Grundkötter-Stock, S. Steinhauer, D. Lentz, H. Puschmann, S. Grabowsky, Accurate crystal structures and chemical properties from NoSpherA2, Chem. Sci. 12 (2021) 1675–1692, https://doi.org/10.1039/D0SC05526C.
[34] F. Neese, The ORCA program system, WIREs Comput. Mol. Sci. 2 (2012) 73–78, https://doi.org/10.1002/wcms.81.
[35] F. Neese, Software update: the ORCA program system, version 4.0, WIREs Comput. Mol. Sci. 8 (2018) e1327, https://doi.org/10.1002/wcms.1327.
[36] R. Dennington, T.A. Keith, J.M. Millam, GaussView, Version 6.1 Semichem Inc. (2016) Shawnee Mission, KS.
[37] M.J. Frisch, G.W. Trucks, H.B. Schlegel, G.E. Scuseria, M.A. Robb, J.R. Cheeseman, G. Scalmani, V. Barone, G.A. Petersson, H. Nakatsuji, X. Li, M. Caricato, A. V. Marenich, J. Bloino, B.G. Janesko, R. Gomperts, B. Mennucci, H.P. Hratchian, J. V. Ortiz, A.F. Izmaylov, J.L. Sonnenberg, D. Williams-Young, F. Ding, F. Lipparini, F. Egidi, J. Goings, B. Peng, A. Petrone, T. Henderson, D. Ranasinghe, V. G. Zakrzewski, J. Gao, N. Rega, G. Zheng, W. Liang, M. Hada, M. Ehara, K. Toyota, R. Fukuda, J. Hasegawa, M. Ishida, T. Nakajima, Y. Honda, O. Kitao, H. Nakai, T. Vreven, K. Throssell, J.A. Montgomery Jr., J.E. Peralta, F. Ogliaro, M. J. Bearpark, J.J. Heyd, E.N. Brothers, K.N. Kudin, V.N. Staroverov, T.A. Keith, R. Kobayashi, J. Normand, K. Raghavachari, A.P. Rendell, J.C. Burant, S.S. Iyengar, J. Tomasi, M. Cossi, J.M. Millam, M. Klene, C. Adamo, R. Cammi, J.W. Ochterski, R.L. Martin, K. Morokuma, O. Farkas, J.B. Foresman, D.J. Fox, Gaussian 16, Revision C.01, Gaussian, Inc., Wallingford CT, 2016.
[38] E.D. Glendening, F. Weinhold, Pauling's conceptions of hybridization and resonance in modern quantum chemistry, Molecules 26 (2021) 4110, https://doi.org/10.3390/molecules26144110.
[39] T. Lu, F.J. Chen, Multiwfn: A multifunctional wavefunction analyzer, Comput. Chem. 33 (2012) 580–592, https://doi.org/10.1002/jcc.22885.
[40] C. Lefebvre, G. Rubez, H. Khartabil, J.-C. Boisson, J. Contreras-García, E. Hénon, Accurately extracting the signature of intermolecular interactions present in the NCI plot of the reduced density gradient *versus* electron density, Phys. Chem. Chem. Phys. 19 (2017) 17928–17936, https://doi.org/10.1039/C7CP02110K.
[41] J. Klein, H. Khartabil, J.C. Boisson, J. Contreras-García, J.-P. Piquemal, E. Hénon, New way for probing bond strength, J. Phys. Chem. A 124 (2020) 1850–1860, https://doi.org/10.1021/acs.jpca.9b09845.
[42] I. Mayer, P. Salvador, Overlap populations, bond orders and valences for 'fuzzy' atoms, Chem. Phys. Lett. 383 (2004) 368–375, https://doi.org/10.1016/j.cplett.2003.11.048.
[43] R.F.W. Bader, A quantum theory of molecular structure and its applications, Chem. Rev. 91 (1991) 893–928, https://doi.org/10.1021/cr00005a013.
[44] R.G. Parr, W. Yang, Density functional approach to the frontier-electron theory of chemical reactivity, J. Am. Chem. Soc. 106 (1984) 4049–4050, https://doi.org/10.1021/ja00326a036.
[45] C. Morell, A. Grand, A. Toro-Labbé, New dual descriptor for chemical reactivity, J. Phys. Chem. A 109 (2005) 205–212, https://doi.org/10.1021/jp046577a.
[46] S.J. Clark, M.D. Segall, C.J. Pickard, P.J. Hasnip, M.J. Probert, K. Refson, M. C. Payne, First principles methods using CASTEP, Z. Kristallogr. 220 (2005) 567–570, https://doi.org/10.1524/zkri.220.5.567.65075.
[47] E.R. Johnson, S. Keinan, P. Mori-Sánchez, J. Contreras-García, A.J. Cohen, W. Yang, Revealing Noncovalent Interactions, J. Am. Chem. Soc. 132 (2010) 6498–6506, https://doi.org/10.1021/ja100936w.
[48] W. Humphrey, A. Dalke, K. Schulten, VMD—visual molecular dynamics, J. Mol. Graph. 14 (1996) 33–38, https://doi.org/10.1016/0263-7855(96)00018-5.
[49] C.F. Matta, J. Hernández-Trujillo, T.-H. Tang, R.F.W. Bader, Hydrogen–hydrogen bonding: a stabilizing interaction in molecules and crystals, Chem. Eur. J. 9 (2003) 1940–1951, https://doi.org/10.1002/chem.200204626.
[50] M.C. Etter, J.C. MacDonald, J. Bernstein, Graph-set analysis of hydrogen-bond patterns in organic crystals, Acta Crystallogr. B 46 (1990) 256–262, https://doi.org/10.1107/s0108768189012929.
[51] Z.-D. Lin, W. Zeng, Aqua-bis-(2-formyl-6-methoxyphenolato)copper(II), Acta Crystallogr. E 62 (2006) m1074–m1076, https://doi.org/10.1107/S1600536806013559.
[52] M. Odabaşoğlu, F. Arslan, H. Ölmez, O. Büyükgüngör, Synthesis, crystal structures and spectral characterization of trans-bisaquabis(o-vanillinato)copper(II), cis-aquabis(o-vanillinato)copper(II) and aqua[bis(o-vanillinato)-1,2-ethylenediimin] copper(II), Dyes Pigm. 75 (2007) 507–515, https://doi.org/10.1016/j.dyepig.2006.06.033.
[53] W. Kristof, G. Zundel, Structurally symmetrical, easily polarizable hydrogen bonds between side chains in proteins and proton-conducting mechanisms. III, Biopolymers 19 (1980) 1753–1769, https://doi.org/10.1002/bip.1980.360191006.
[54] G. Zundel, B. Brzeziński, Hydrogen-bonded chains with large proton polarizability due to collective proton motion - pathways for protons in biological membranes, Pol. J. Chem. 72 (1998) 172–192.
[55] K. Baranowska, N. Piwowarska, A. Herman, A. Dołęga, Imidazolium silanethiolates relevant to the active site of cysteine proteases. Cooperative effect in a chain of NH^{+}—S^{-} hydrogen bonds, New J. Chem. 36 (2012) 1574–1582, https://doi.org/10.1039/C2NJ40114B.
[56] S. Chaiwongwattana, M. Phonyiem, V. Vchirawongkwin, S. Prueksaaroon, K. Sagarik, Dynamics and mechanism of structural diffusion in linear hydrogen bond, J. Comput. Chem. 33 (2012) 175–188, https://doi.org/10.1002/jcc.21957.
[57] J.H. Hack, J.P. Dombrowski, X. Ma, Y. Chen, N.H.C. Lewis, W.B. Carpenter, C. Li, G.A. Voth, H.H. Kung, A. Tokmakoff, Structural characterization of protonated water clusters confined in HZSM-5 zeolites, J. Am. Chem. Soc. 143 (2021) 10203–10213, https://doi.org/10.1021/jacs.1c03205.
[58] J.I. Martínez-Araya, Why is the dual descriptor a more accurate local reactivity descriptor than fukui functions? J. Math. Chem. 53 (2015) 451–465, https://doi.org/10.1007/s10910-014-0437-7.